INORGANIC CHEMISTRY FRONTIERS

RESEARCH ARTICLE

View Article Online
View Journal | View Issue

Cite this: *Inorg. Chem. Front.*, 2024, **11**, 2626

Synthesis and characterization of a $CsPbCl_3$ perovskite doped with Nd^{3+}: structural, optical, and energy transfer properties

Mariusz Stefanski, *[a] Bartosz Bondzior,[a] Adam Basinski,[a] Maciej Ptak,[a] Bibo Lou[b] and Chong-Geng Ma[b]

Received 18th January 2024,
Accepted 18th March 2024

DOI: 10.1039/d4qi00171k

rsc.li/frontiers-inorganic

The purpose of this paper is to synthesize a micrometric inorganic perovskite $CsPbCl_3$:Nd^{3+} and investigate the impact of doping with rare-earth ions on structural and optical properties, as well as energy transfer pathways between the host and dopant. Herein, we report the solid-state reaction synthesis of a concentration series of $CsPbCl_3$:x%Nd^{3+} annealed under a nitrogen atmosphere. Additional doping of a material that already exhibits luminescence with an optically active ion increases its application potential. Structural features were determined using X-ray powder diffraction and Raman spectroscopy. Morphology studies performed with scanning electron microscopy revealed micrometric, well-separated cubic-like crystallites with a good distribution of individual elements. Surprisingly, a photoluminescence (PL) study showed that only blue emission appears when the material is excited with a diode operating in the UV range. Apparently, the emission of Nd^{3+} ions can only be obtained with direct excitation of the lanthanide. The photoluminescence excitation (PLE) spectrum monitored for Nd^{3+} emission confirmed the lack of energy transfer between the host and dopant. Possible explanations for this behavior have been put forth and substantiated by the first-principles electronic structure calculations in the framework of hybrid density functional theory.

Introduction

Perovskite halides (chlorides, iodides, and bromides) are popular choices for nanocrystalline optoelectronic materials due to their simple synthesis route and efficient tunable luminescence. The research on perovskite halides as luminescent materials has been conducted extensively due to the broadband host emission believed to originate from the coupling of the excited carriers with distorted lead halide units.[1] This origin of the luminescence of halide perovskites is responsible for high quantum yield and provides the possibility of material optimization by doping with either optically active[2] or inactive ions,[3] by means of bandgap engineering. Cesium lead chloride with the chemical formula $CsPbCl_3$ is a member of the all-inorganic halide perovskite family and has attracted significant attention in the scientific community due to its high efficiency and stability compared to its organic–inorganic counterparts. The choice of the synthesis method can affect the quality, size, and morphology of the resulting samples, influencing their optoelectronic properties and potential applications. The development of efficient and reproducible synthesis methods is crucial for the widespread use of the $CsPbCl_3$ perovskite in various optoelectronic applications.

Recent research on perovskite nanocrystals and thin films has focused on improving the stability and efficiency of $CsPbCl_3$ perovskite solar cells.[4,5] Moreover, the $CsPbCl_3$ perovskite has shown potential in other optoelectronic applications, such as light-emitting diodes (LEDs)[6] or as an element of a phosphor–glass composite.[7] Overall, the $CsPbCl_3$ perovskite has demonstrated great potential as a candidate for high-performance and stable optoelectronic devices. It has also recently been studied extensively as a nanocrystal host for rare earth and transition metal dopants. Since the 1990s, it has also been known for exhibiting free exciton emission in the UV region under high-intensity excitation.[8,9] This exciton state has been used as a sensitizer to enhance the dopant's emission.[10] It can be noted that the literature considering nanometric inorganic halide perovskites is quite rich, but studies involving larger analogs are still very limited. $CsPbCl_3$ quantum dots have been reported to exhibit efficient blue-violet emission under UV excitation.[11] A recent study investigated the structural and spectroscopic properties of micrometric

[a]*Institute of Low Temperature and Structure Research, Polish Academy of Sciences, 50-422 Wroclaw, Poland. E-mail: m.stefanski@intibs.pl*
[b]*School of Optoelectronic Engineering and CQUPT-BUL Innovation Institute, Chongqing University of Posts and Telecommunications, No. 2 Chongwen Road, Nan'an District, Chongqing 400065, China*

$CsPbCl_3$ perovskite powders doped with Yb^{3+} ions, with varying dopant concentrations (1–20%) prepared *via* a simpler solid-state reaction route. Compared to quantum dots, micrometric $CsPbCl_3$ can be prepared *via* a solid-state reaction route and exhibit blue emission.[12] The study illustrates that similar to other lead halides, the $CsPbCl_3$ host is expected to transfer energy to the RE dopant.[2] Our current study demonstrates this assumption to be inaccurate for some RE dopants.

Nd^{3+} has a characteristic emission spectrum that includes sharp lines in the near-infrared region, with emission peaks at around 880 nm, 1060 nm, and 1330 nm. The emission intensity and lifetime of Nd^{3+} luminescence are highly dependent on the local crystal field environment, which can be tailored by doping the ion into different host materials. Nd^{3+} exhibits a fluorescence lifetime, which can range from microseconds to milliseconds, making it ideal for applications such as solid-state lasers,[13] where the neodymium ions act as an active medium, producing high-power laser emissions. These materials also find applications in optical amplifiers, fiber optic communication,[14] and biological imaging.[15] Due to the fact that the ionic radius of Nd^{3+} ions is smaller (99.5 pm) than that of Pb^{2+} ions (119 pm),[16] they can be doped in higher concentrations without changing the structure of $CsPbCl_3$.

Recently Xiong *et al.* investigated $CsPbCl_3$:Nd^{3+},[17] where the dopant was used not as a luminescent center but rather as an enhancement agent for exciton emission. Another study reported the spectroscopic properties of Mn^{2+}- and Nd^{3+}-co-doped $CsPbCl_3$.[18] To the best of our knowledge, no luminescence of Nd^{3+} ions in $CsPbCl_3$ upon direct excitation of the dopant was reported. In this paper, we report the structure, morphology, and luminescence properties of a concentration series of $CsPbCl_3$:Nd^{3+} microcrystals synthesized by a solid-state reaction method. Additionally, we provide an explanation for the absence of energy transfer between the host and the dopant, supported by first-principles calculations using a hybrid density functional model.

Results and discussion

Structural and thermal properties

Fig. 1a shows the XRD patterns of a concentration series of $CsPbCl_3$ perovskite powders doped with Nd^{3+} ions. Analysis of the diffractograms confirmed that the studied host can accommodate a maximum of 20% dopant without structural disruption. A further increase in the concentration of Nd^{3+} ions caused the appearance of foreign peaks, inconsistent with pattern #243734. Therefore, the $CsPbCl_3$:25%Nd^{3+} sample was not considered in further investigations. The pure phase samples exhibited an orthorhombic structure belonging to the *Pnma* space group. Fig. 1b presents a simplified diagram of a $CsPbCl_3$ unit cell containing only lead atoms. The studied material reveals a distance between Pb ions, partially substituted by Nd,[19] reaching more than 5 Å, which ensures a low concentration quenching rate.

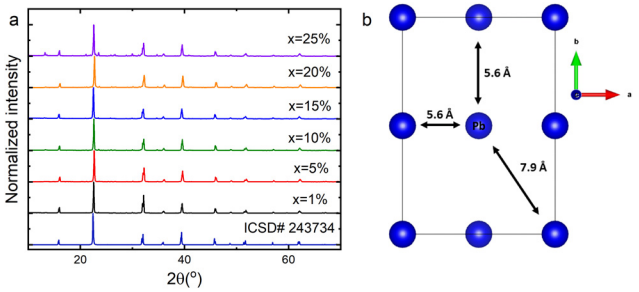

Fig. 1 X-ray diffraction patterns of the $CsPbCl_3$:*x*%Nd^{3+} perovskite powders (a) and a simplified unit cell scheme of an undoped sample (b).

To validate the thermal stability of the studied perovskites, we performed thermogravimetric analysis for powders containing 1 and 20% of Nd^{3+} ions (Fig. 2). The decomposition of the sample with a lower concentration begins at around 840 K. Increasing the dopant ion concentration to 20% lowers the degradation threshold to 825 K. In both cases, degradation ends at around 1200 K. The differences in the weight loss suggest that metallic neodymium is the final form. Fig. 3 shows the scanning electron microscopy (SEM) images of the morphology of $CsPbCl_3$ perovskite powders doped with Nd^{3+}. It can be observed that the investigated host shows well-developed crystallites with a polyhedron shape, sharp boundaries

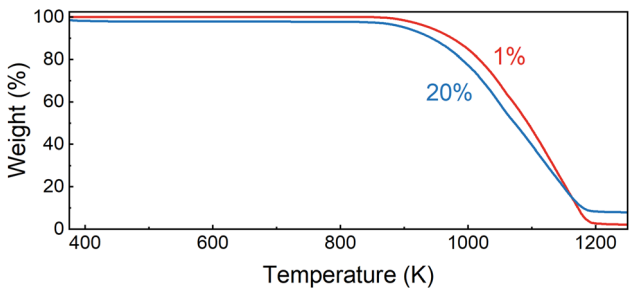

Fig. 2 TGA curves for $CsPbCl_3$ powders composed of 1 and 20% of Nd^{3+} ions.

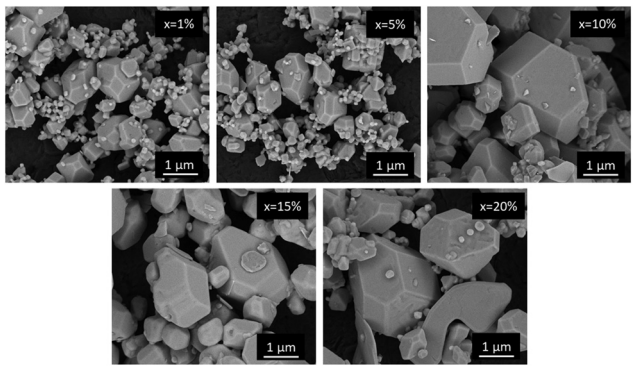

Fig. 3 SEM images of the $CsPbCl_3$ perovskite powders containing different concentrations of Nd^{3+} ions.

and different sizes with a dominant micrometric fraction. It is worth noting that even a 20% dopant ion content does not affect the quality of the obtained crystallites. The situation is different in comparison with $CsPbCl_3$ doped with Yb^{3+} ions synthesized using the same technique.[20] In the latter case, the strongly doped samples (more than 10%) had blurred grain boundaries and their aggregation was very advanced, which significantly affected their optical properties.

In order to check the distribution of individual elements, EDS mapping for a $CsPbCl_3$:10%Nd^{3+} ion was performed and is presented in Fig. 4. It is proven that the elements are evenly distributed throughout the crystallite volume and the incorporation of Nd^{3+} was successful.

Raman spectra

Fig. 5 illustrates the Raman spectra of all examined powders. All spectra exhibit four bands with maxima at about 24, 36, 114, and 199 cm^{-1}, as well as two shoulders at roughly 57 and 104 cm^{-1} at ambient temperature. The recorded spectra match well the data reported in the literature for the orthorhombic phase of $CsPbCl_3$ and demonstrate that the structure is maintained over the whole concentration range.[21,22] Raman bands become narrow and well-spaced at 80 K, with peaks at 30, 35, 41, 51, 71, 88, 109, 120, and 201 cm^{-1} for x = 1%. At both temperatures, an increased dopant ion concentration induces band broadening and an intensity decrease, which are connected to the increased concentration of defects generated by substitution. This impact is most prominent under ambient conditions for bands in the 100–120 cm^{-1} range, with a strong contribution from Cs^+ ion movements.[21,22] The relative change in the intensity of this band decreases exponentially as the dopant ion concentration increases, demonstrating successful substitution with Nd^{3+} ions in the crystal structure. The concentration-related broadening of bands associated with longer phonon lifetimes becomes more apparent after cooling. Band shifts caused by various masses and radii of Pb^{2+} and Nd^{3+} ions are noticeable in addition to the observed widening. The strongest of these, ranging up to around 2.3 cm^{-1}, are connected with the vibrations of $PbCl_6$ octahedra in the 70–90 cm^{-1} range.[21,22]

Optical properties

The diffuse reflectance spectra of a concentration series of $CsPbCl_3$ perovskite powders doped with Nd^{3+} ions cover the range of the UV-VIS-NIR region as presented in Fig. 6a. It exhibits a strong band in the range of 200–400 nm corresponding to the absorption of the host.[23] An exciton band at the absorption edge flattens out as the concentration of Nd^{3+} ions increases (Fig. 6b). In the visible and infrared spectral ranges, less intense absorption bands originating from Nd^{3+} f–f transitions can be observed.[24] Diffuse reflectance spectra were used to determine the size of the energy band gap (E_g) in $CsPbCl_3$:x%Nd^{3+} perovskite powders by the Kubelka–Munk method:

$$F(R) = \frac{(1-R)^2}{2R} \quad (1)$$

where R is the reflectance. The band gap energies were extrapolated from the intercept of the fitted straight line at $F(R) = 0$ in the $F(h\nu)^{1/2}$ *versus* the energy ($h\nu$) plot. The calculation results can be found in Fig. 6c. It was found that the energy gap is of the order of 2.9 eV and reaches the highest value for the material containing the smallest concentration of the dopant. Our first-principles calculations confirmed a gap of 2.93 eV between the host's valence band (VB) and the conduction band (CB), as illustrated in Fig. 9, providing further support for this experimental determination.

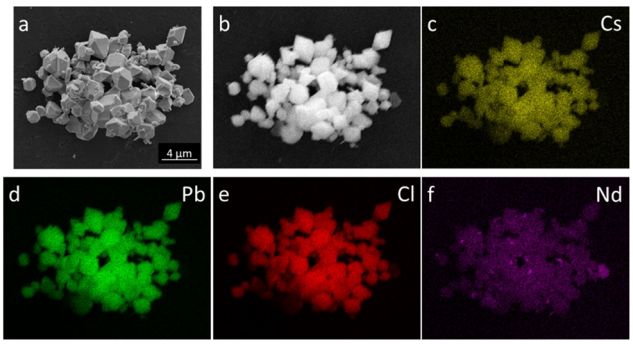

Fig. 4 SEM image (a) and EDS elemental mapping (b–f) of the $CsPbCl_3$:10%Nd^{3+} perovskite powder.

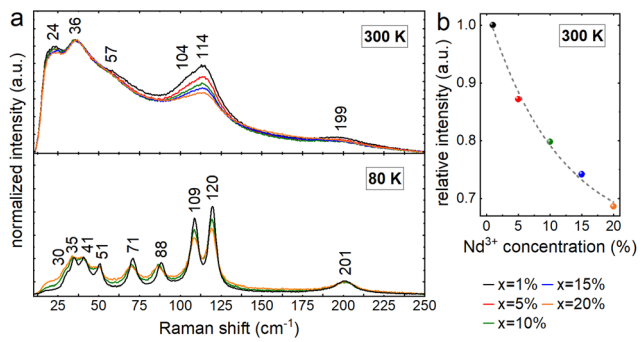

Fig. 5 Raman spectra of the $CsPbCl_3$ perovskite powders containing different concentrations of Nd^{3+} ions at 300 and 80 K (a) together with the relative intensity change of the band at 114 cm^{-1} at 300 K (b).

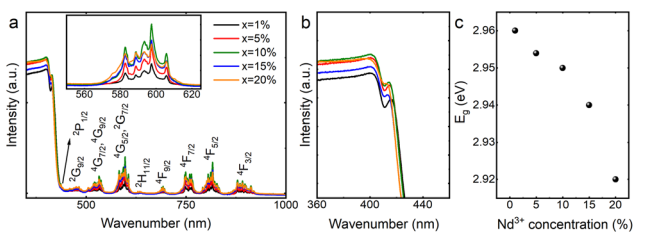

Fig. 6 Diffuse reflectance spectra of the $CsPbCl_3$:x%Nd^{3+} perovskite powders (a) together with an enlarged spectrum showing the exciton band (b) and energy gap values as a function of dopant concentration (c).

The excitation spectrum of $CsPbCl_3$:20%Nd^{3+} was recorded and is shown in Fig. 7a. It can be seen that by monitoring the wavelength of 1061 nm, conventional f–f transitions of Nd^{3+} ions were observed, identical to those in the visible to NIR range of the absorption spectrum (Fig. 6); however, in the ultraviolet range (300–400 nm), no band originating from the host was detected, indicating a lack of energy transfer between the host and the dopant. It is worth mentioning that there are not many reports in the literature on $CsPbCl_3$ doped with Nd^{3+} ions. It is probably due to the lack of energy transfer, which greatly limits its potential applications and makes this material unattractive. Recently, a paper reporting emission from Nd^{3+} ions in $CsPbCl_3$ under 365 nm excitation was published.[18] However, in that case, Mn^{2+} ions were introduced into the crystal structure of the host, which provided a bridge for energy transfer between the matrix and the Nd^{3+} ions.

The emission spectra of a concentration series of $CsPbCl_3$ perovskite powders doped with Nd^{3+} ions recorded at liquid nitrogen temperature are depicted in Fig. 7b. Experiments at 80 K were required because the luminescence of the exciton was completely quenched at 300 K. It is also worth noting that the spectra in the visible range were recorded upon 360 nm excitation, while the spectra in the infrared range were collected under 808 nm excitation. The measurement system was designed to expose the sample to two different beams at the same time, while the detector recorded the signal continuously in the range of 350–1100 nm. This arrangement made it possible to merge both spectra. The use of two excitation sources was necessary because it turned out that no energy transfer to Nd^{3+} ions was observed when the sample was excited into the host's conduction band (Fig. 7a). Regardless of the concentration of dopant ions, the analyzed materials revealed exciton bands in the visible range, the maxima of which are located at about 416 nm, while in the infrared range, two bands of Nd^{3+} ions were visible, whose emission maxima are located at 882 nm and 1060 nm, assigned to $^4F_{3/2} \rightarrow {}^4I_{9/2}$ and $^4F_{3/2} \rightarrow {}^4I_{11/2}$ transitions, respectively.[25] In order to indirectly compare the emission intensities of Nd^{3+} ions, the spectra shown in Fig. 7b were normalized relative to the exciton intensity and their relative intensities are plotted in Fig. 7c. It can be clearly seen that as the dopant concentration increases, the Nd^{3+} emission intensity also increases, and the concentration quenching,[26] typical of this lanthanide usually occurring by a cross-relaxation process, is not observed. In fact, the opposite situation happens. The intensity of the $CsPbCl_3$:20%Nd^{3+} sample is so high that showing it in the same figure as the other samples required an additional scale. The lack of concentration quenching is probably related to the large Nd^{3+}–Nd^{3+} distances (partially substituted lead positions due to its similar size and smaller charge mismatch compared to cesium[27]) in the unit cell presented in Fig. 1b. A minimal shift of the maximum of the exciton's absorption bands toward higher energies is observed. This is related to a slight reduction in the unit cell volume of $CsPbCl_3$:Nd^{3+} as a consequence of the substitution of the larger (Pb^{2+}) ion with a smaller one (Nd^{3+}), which is consistent with the quantum confinement effect.[28,29] A similar behavior was reported earlier in the literature.[17]

Fig. 8 shows the luminescence kinetics of the investigated compounds measured under 360 nm and 808 nm excitation and monitoring of the emission maximum of the exciton (Fig. 8a) and Nd^{3+} ions (Fig. 8b), respectively. It is worth noting that depending on the monitored band, measurements at different temperatures were made due to hardware limits. Unfortunately, the Nd^{3+} emission intensity of the sample containing 1% dopant was below the detection capabilities of the

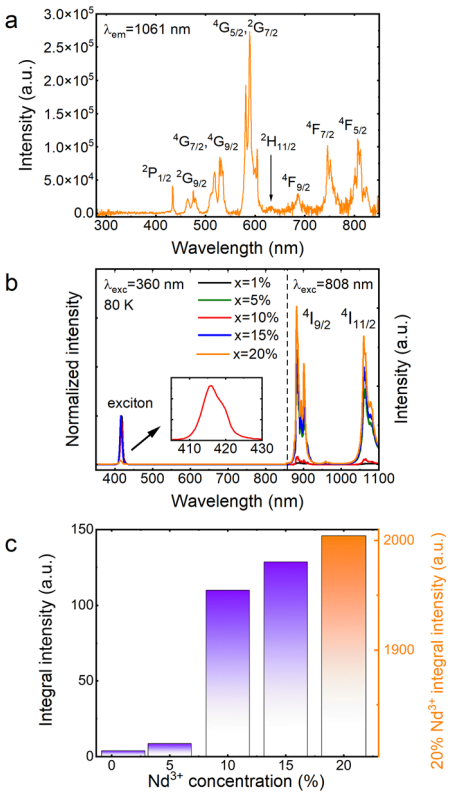

Fig. 7 Excitation spectra of $CsPbCl_3$:20%Nd^{3+} at 300 K (a). Emission spectra of the $CsPbCl_3$:*x*%Nd^{3+} perovskite powders recorded at 80 K together with an inset showing an enlarged exciton spectrum of the $CsPbCl_3$:10%Nd^{3+} sample (b), and integral intensities of Nd^{3+} emission (c). For clarity in (c), the sample containing 20% of the dopant is shown on a larger scale.

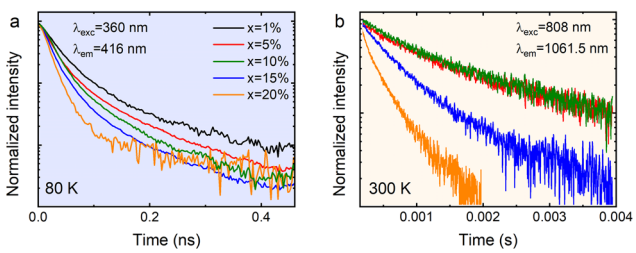

Fig. 8 The luminescence decay profiles of the exciton (a) and Nd^{3+} (b) luminescence in $CsPbCl_3$:*x*%Nd^{3+} perovskite powders.

measurement system; therefore, recording its profile was impossible. Nevertheless, it can be observed that all of the measured curves show a bi-exponential nature. In the case of an exciton, this can be attributed to the presence of free and bound excitons (the asymmetrical shape of the band shown in the inset of Fig. 7b [20]). However, in the case of dopant ions, some non-radiative processes may be responsible for such behavior. It can be clearly seen that as the Nd^{3+} concentration increases, the deviation from the exponential characteristics of the profiles becomes more pronounced. The luminescence profiles of $CsPbCl_3$:x%Nd^{3+} were well matched using a double exponential function:

$$I(t) = A_1 \exp\left(-\frac{t}{\tau_1}\right) + A_2 \exp\left(-\frac{t}{\tau_2}\right), \quad (2)$$

where $I(t)$ means the emission intensity, A_1 and A_2 are the fitting constants and τ_1 and τ_2 stand for their corresponding lifetimes. The average lifetimes (t_{av}) were determined using eqn (3) and are presented in Table 1. It turned out that the luminescence decays of excitons observed in the investigated material are shorter than those already reported for $CsPbCl_3$ doped with transition metals or lanthanides obtained in the form of nanocrystalline colloids or films.[30–33]

$$t_{av} = \frac{A_1\tau_1^2 + A_2\tau_2^2}{A_1\tau_1 + A_2\tau_2} \quad (3)$$

It seems that the mechanism responsible for the generation of exciton luminescence in $CsPbCl_3$:Nd^{3+} is similar to that presented by us earlier for the same host but doped with Yb^{3+} ions.[20] In this case, as in the previous one, there is also an asymmetric emission band in the visible range upon excitation with a 360 nm line (inset in Fig. 7b), which indicates the emission of a free exciton (FE) and bound exciton (BE) on the defect simultaneously after the prior population of the host conduction band. However, in the analog containing Nd^{3+}, there was no energy transfer between the host and dopant ions, as they appear relatively isolated from each other. The reduction of the Nd^{3+} emission lifetime is observed in samples with a dopant concentration above 10%. Given the fact that the possibility of concentration quenching was excluded by the increasing intensity as a function of concentration, such a reduction in lifetimes can be related to the appearance of surface defects due to heavy doping with lanthanide ions.

Fig. 9 shows the calculated density of states of the $CsPbCl_3$:Nd^{3+} system. For the pristine host, the top of the valence bands is dominated by the Pb-s and Cl-p orbitals, and the bottom of the conduction bands is dominated by the Pb-p orbitals. With the doping of Nd^{3+} ions, the top of the valence bands is hardly influenced, while the bottom of the conduction bands is greatly hybridized by the Nd-4f orbitals. Our first-principles calculations demonstrate that the ground state $^4I_{9/2}$ of Nd^{3+} ions in $CsPbCl_3$ lies 3.88 eV below the top of the host's VB, as illustrated in Fig. 9. The energy positions of Nd^{3+} dopants are greatly influenced by the properties of hosts, as the variation of the vacuum-referred binding energy of the 4f level is no more than 0.4 eV for inorganic compounds.[34] Here, the halide anions exhibit less Pauling electronegativity than the oxygen anion, and the top of the valence bands was greatly hybridized by the Pd-s orbitals, which makes the vacuum-referred binding energy of the valence bands higher than those of the oxides. As a result, the excited energy levels of Nd^{3+} ions, considering the multiplets up to $^4D_{3/2}$ obtained from Dieke's diagram, are entirely buried within the VB and

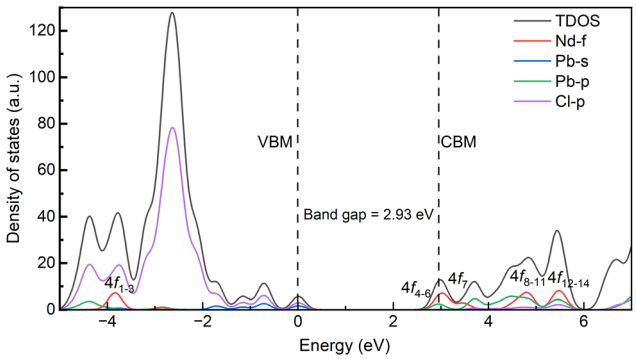

Fig. 9 Density of state diagrams calculated for $CsPbCl_3$:Nd^{3+}. The labels VBM and CBM represent the maximum of the valence band and the minimum of the conduction band, respectively. The positions of the fourteen 4f dopant energy states are denoted by $4f_n$ (n = 1–14).

Table 1 The lifetimes of the excitons and Nd^{3+} ions calculated by fitting the decays with the double-excitation function

Dopant content	Exciton lifetime (80 K)	Neodymium lifetime (300 K)
1%	53 ps	
5%	47 ps	2.15 ms
10%	46 ps	1.93 ms
15%	31 ps	0.86 ms
20%	28 ps	0.19 ms

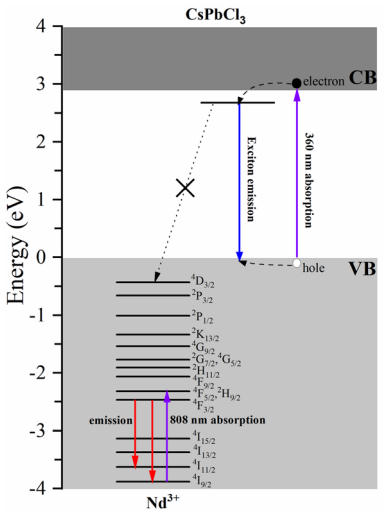

Fig. 10 Electronic energy level scheme determined for the $CsPbCl_3$:Nd^{3+} perovskite powder.

are unable to accept carriers from the host. Moreover, the energy mismatch between the exciton energy and the energy separation between Nd^{3+} multiplets exacerbates the hindrance of energy transfer. These factors, as depicted in Fig. 10, effectively block any energy transfer from the host to Nd^{3+} dopants. Therefore, the only way to obtain luminescence from Nd^{3+} ions in the investigated host is to excite them directly using, for example, an 808 nm line.

Conclusions

Systematic structural and optical studies considering a micrometric $CsPbCl_3$ perovskite containing Nd^{3+} ions with concentrations in the range of 1–25% have been reported. Powdered samples were prepared using the classical solid state reaction method. XRD diffractograms and Raman spectra proved that the investigated materials exhibit an orthorhombic *Pnma* symmetry and do not show additional phases originating from impurities when the dopant concentration does not exceed 20%. TGA analysis revealed that the investigated materials are highly thermally stable. SEM images confirmed the micrometric size of the $CsPbCl_3$:Nd^{3+} crystallites and elemental mapping showed that the dopant is homogeneously distributed throughout the sample volume. Diffuse reflectance spectra indicated strong absorption in the UV range and typical Nd^{3+} ion transitions in $CsPbCl_3$. It turned out that the magnitude of the energy gap is of the order of 2.96 eV and gently decreases with increasing dopant concentration. Studies of optical properties revealed that by excitation of the host conduction band, only exciton luminescence can be obtained. In order to produce emission from Nd^{3+} ions, direct excitation is required. The reliability of the measured host band gap was confirmed through our first-principles calculations. The calculations further demonstrate that the electronic energy levels of the excitons remain isolated from those of Nd^{3+} ions, thereby indicating the absence of energy transfer between them.

Experimental

Chemicals

The concentration series of $CsPb_{1-x}Nd_xCl_3$ (x = 1, 5, 10, 15, 20, and 25 mol%) perovskite powder was obtained *via* the solid-state reaction route. Stoichiometric amounts of the following precursors: CsCl (Sigma-Aldrich, 99.9%), $PbCl_2$ (Sigma-Aldrich, 98%) and $NdCl_3{\cdot}6H_2O$ (Sigma-Aldrich, 99.9%) were weighed and mixed vigorously in an agate mortar in the presence of CH_3OH. Alcohol was added solely to provide a better environment for mixing the reactants, which is crucial in solid-state synthesis to achieve an even distribution of components. After thorough mixing and evaporation of CH_3OH, the obtained powder was moved to a quartz boat and placed in a tube furnace. The heating process was carried out according to the same regime as reported previously[12,20] under a nitrogen flow. The dopant content was determined based on theoretical calculations.

Measurement methods

The X-ray diffraction (XRD) pattern was measured using an X'Pert PRO powder diffractometer (PANalytical, The Netherlands) equipped with a linear PIXcel detector and using Cu-Kα radiation (λ = 1.54056 Å). A PerkinElmer TGA 4000 was used to perform thermogravimetric analysis (TGA) on samples containing 1 and 20% of Nd^{3+} ions at temperatures ranging from 300 to 1250 K. The samples weighed 91.88 and 60.63 mg, respectively, and a 10 K min^{-1} heating rate was used. Nitrogen was used as a purging gas. The chemical composition and general morphology of the samples were checked using a FE-SEM microscope (FEI Nova NanoSEM 230) equipped with an EDS analyzer (EDAX Genesis XM4). Raman spectra at room temperature and 80 K were recorded in the 10–300 cm^{-1} range using a Renishaw InVia Raman spectrometer equipped with a confocal DM 2500 Leica optical microscope, a thermoelectrically cooled CCD as a detector and a laser operating at 830 nm. The absorption measurements were performed in the back scattering mode using an Agilent Cary 5000 spectrophotometer. The excitation spectrum was recorded using a FLS1000 fluorescence spectrometer from Edinburgh Instruments. Low-temperature emission spectra were recorded with a Hamamatsu photonic multichannel analyzer PMA-12 equipped with a BT-CCD linear image sensor. The laser diode operating under 360 nm and 808 nm was applied as an excitation source. The temperature of the samples during emission measurements was controlled by using a Linkam THMS600 heating/freezing stage. The luminescence decay profiles of the excitons were recorded using a femtosecond laser (Coherent Model Libra). The luminescence decay profiles of Nd^{3+} emission were recorded using the McPherson spectrometer with a Hamamatsu R955 photomultiplier and a digital oscilloscope Tektronix MDO3052, as well as a Nd:YAG-pumped Ti-sapphire tunable pulse laser.

Computational method

The first-principles calculations were performed utilizing the Vienna *ab initio* simulation package,[35] employing the projector augmented wave method in conjunction with density functional theory (DFT). To accurately capture the electronic properties of Pb-based halide perovskites, the PBE0 hybrid functional with 25% of non-local Fock exchange[36] was adopted, along with the consideration of the spin–orbit coupling interaction, following the recommendation of ref. 37. The valence configurations of Nd, Cs, Pb and Cl were determined as $5s^25p^66s^24f^4$, $5s^25p^66s^1$, $5d^{10}6s^26p^2$ and $3s^23p^5$, respectively. The dopant effect of Nd^{3+} ions was modeled in the 2 × 2 × 2 supercell, where one Pb^{2+} ion was substituted by one Nd^{3+} ion. For the pure and doped systems, the closed-shell and spin-polarized DFT calculation forms were applied, respectively. The plane-wave basis cutoff energy was set to 500 eV, with the convergence criteria of 10^{-5} eV for electronic energy minimization and 0.02 eV $Å^{-1}$ for Hellmann–Feynman forces on each

atom. A 6 × 6 × 6 *k*-point mesh based on the Monkhorst–Pack scheme was employed for the pure $CsPbCl_3$ host, while a single *k* point at *Γ* was utilized for all the supercells.

Data availability

The data presented in this study are openly available in Zenodo at DOI: 10.5281/zenodo.8207373.

Conflicts of interest

There are no conflicts to declare.

Acknowledgements

This research was funded by the National Science Center, Poland, grant no. NCN-2021/43/D/ST5/01865. C.G. Ma acknowledges the support from the National Natural Science Foundation of China (Grant No. 52161135110 and 12274048). BL acknowledges the support from the Scientific and Technological Research Program of the Chongqing Municipal Education Commission (Grant No. KJQN202200629). The authors thank Professor Marek Drozd for performing the thermogravimetric measurements.

References

1 Y. Zhou, Z. J. Yong, K. C. Zhang, B. M. Liu, Z. W. Wang, J. S. Hou, Y. Z. Fang, Y. Zhou, H. T. Sun and B. Song, Ultrabroad Photoluminescence and Electroluminescence at New Wavelengths from Doped Organometal Halide Perovskites, *J. Phys. Chem. Lett.*, 2016, **7**, 2735–2741.

2 Y. Zhou, J. Chen, O. M. Bakr and H. T. Sun, Metal-Doped Lead Halide Perovskites: Synthesis, Properties, and Optoelectronic Applications, *Chem. Mater.*, 2018, **30**, 6589–6613.

3 Z. J. Yong, S. Q. Guo, J. P. Ma, J. Y. Zhang, Z. Y. Li, Y. M. Chen, B. Bin Zhang, Y. Zhou, J. Shu, J. L. Gu, L. R. Zheng, O. M. Bakr and H. T. Sun, Doping-Enhanced Short-Range Order of Perovskite Nanocrystals for Near-Unity Violet Luminescence Quantum Yield, *J. Am. Chem. Soc.*, 2018, **140**, 9942–9951.

4 A. Ishii and T. Miyasaka, Quantum cutting-induced near-infrared luminescence of Yb^{3+} and Er^{3+} in a layer structured perovskite film, *J. Chem. Phys.*, 2020, **153**, 194704.

5 J. Jiang, Z. Jin, F. Gao, J. Sun, Q. Wang and S. Liu, $CsPbCl_3$-Driven Low-Trap-Density Perovskite Grain Growth for >20% Solar Cell Efficiency, *Adv. Sci.*, 2018, **5**, 1800474.

6 T. Fan, J.-T. Lü, W.-Q. Deng, J.-X. Mai, J. Liang, T.-T. Deng, W. Fan, Q.-S. Zhou and Q.-F. Lin, Orange LED and cell fluorescence imaging of Mn^{2+} doped $CsPbCl_3$ water-soluble nanocrystals with improved stability and optimized luminescence, *Ceram. Int.*, 2023, **49**, 13066–13073.

7 L.-Y. Cao, S.-C. Si, J.-B. Yu, C.-G. Ma, J.-B. Qiu and J. Wang, A precisely space-separated strategy of donor-acceptor for intense red emitting composite borosilicate glass co-doped with $CsPbCl_3$ quantum dots and Mn^{2+} ions, *Chem. Eng. J.*, 2021, **417**, 129177.

8 I. Baltog, S. Lefrant, C. Dimofte and L. Mihut, Phonon assisted excitonic luminescence in $CsPbCl_3$, *Radiat. Eff. Defects Solids*, 1995, **135**, 285–287.

9 I. Baltog, L. Mihut and S. Lefrant, Excitonic luminescence in $CsPbCl_3$ crystals under intense excitation, *J. Lumin.*, 1996, **68**, 271–277.

10 K. Xu and A. Meijerink, Tuning Exciton–Mn^{2+} Energy Transfer in Mixed Halide Perovskite Nanocrystals, *Chem. Mater.*, 2018, **30**, 5346–5352.

11 Y. Liu, G. Pan, R. Wang, H. Shao, H. Wang, W. Xu, H. Cui and H. Song, Considerably enhanced exciton emission of $CsPbCl_3$ perovskite quantum dots by the introduction of potassium and lanthanide ions, *Nanoscale*, 2018, **10**, 14067–14072.

12 M. Stefanski, V. Boiko, M. Ptak and W. Strek, Effect of Yb^{3+} concentration on the optical properties and trap creation in $CsPbCl_3$ perovskite powder, *J. Alloys Compd.*, 2022, **905**, 164216.

13 J. Lu, K. I. Ueda, H. Yagi, T. Yanagitani, Y. Akiyama and A. A. Kaminskii, Neodymium doped yttrium aluminum garnet ($Y_3Al_5O_{12}$) nanocrystalline ceramics - A new generation of solid state laser and optical materials, *J. Alloys Compd.*, 2002, **341**, 220–225.

14 M. Naftaly and A. Jha, Nd^{3+}-doped fluoroaluminate glasses for a 1.3 μm amplifier, *J. Appl. Phys.*, 2000, **87**, 2098.

15 Y.-F. Wang, G.-Y. Liu, L.-D. Sun, J.-W. Xiao, J.-C. Zhou and C.-H. Yan, Nd^{3+}-Sensitized Upconversion Nanophosphors: Efficient In Vivo Bioimaging Probes with Minimized Heating Effect, *ACS Nano*, 2013, **7**, 7200–7206.

16 R. D. Shannon, Revised effective ionic radii in halides and chalcogenides, *Acta Crystallogr., Sect. A: Cryst. Phys., Diffr., Theor. Gen. Crystallogr.*, 1976, **A32**, 751–767.

17 J. Xiong, S. Cao, K. Xing, M. Chen, R. Zeng, B. Zou and J. Zhao, Enhanced photoluminescence efficiencies of $CsPbCl_{3-x}Br_x$ nanocrystals by incorporating neodymium ions, *J. Lumin.*, 2022, **243**, 118658.

18 M. Zeng, F. Locardi, D. Mara, Z. Hens, R. Van Deun and F. Artizzu, Switching on near-infrared light in lanthanide-doped $CsPbCl_3$ perovskite nanocrystals, *Nanoscale*, 2021, **13**, 8118–8125.

19 J. P. Ma, Y. M. Chen, L. M. Zhang, S. Q. Guo, J. D. Liu, H. Li, B. J. Ye, Z. Y. Li, Y. Zhou, B. Bin Zhang, O. M. Bakr, J. Y. Zhang and H. T. Sun, Insights into the local structure of dopants, doping efficiency, and luminescence properties of lanthanide-doped $CsPbCl_3$ perovskite nanocrystals, *J. Mater. Chem. C*, 2019, **7**, 3037–3048.

20 M. Stefanski, M. Ptak, A. Sieradzki and W. Strek, Optical characterization of Yb^{3+}:$CsPbCl_3$ perovskite powder, *Chem. Eng. J.*, 2021, **408**, 127347.

21 M. Liao, B. Shan and M. Li, In Situ Raman Spectroscopic Studies of Thermal Stability of All-Inorganic Cesium Lead

Halide ($CsPbX_3$, X = Cl, Br, I) Perovskite Nanocrystals, *J. Phys. Chem. Lett.*, 2019, **10**, 1217–1225.
22 D. M. Calistru, L. Mihut, S. Lefrant and I. Baltog, Identification of the symmetry of phonon modes in $CsPbCl_3$ in phase IV by Raman and resonance-Raman scattering, *J. Appl. Phys.*, 1997, **82**, 5391–5395.
23 S. Smółka, M. Mączka, D. Drozdowski, D. Stefańska, A. Gągor, A. Sieradzki, J. K. ZarÈ©ba and M. Ptak, Effect of Dimensionality on Photoluminescence and Dielectric Properties of Imidazolium Lead Bromides, *Inorg. Chem.*, 2022, **61**, 15225–15238.
24 A. Miguel, J. Azkargorta, R. Morea, I. Iparraguirre, J. Gonzalo, J. Fernandez and R. Balda, Spectral study of the stimulated emission of Nd^{3+} in fluorotellurite bulk glass, *Opt. Express*, 2013, **21**, 9298–9307.
25 A. R. Molla, A. Tarafder, S. Mukherjee and B. Karmakar, Transparent Nd^{3+}-doped bismuth titanate glass-ceramic nanocomposites: Fabrication and properties, *Opt. Mater. Express*, 2014, **4**, 843–863.
26 T. H. Q. Vu, B. Bondzior, D. Stefańska and P. J. Dereń, Low-temperature optical thermometer based on the luminescence of the double perovskite Ba_2MgWO_6: Nd^{3+}, *J. Lumin.*, 2023, **257**, 119750.
27 G. Pan, X. Bai, D. Yang, X. Chen, P. Jing, S. Qu, L. Zhang, D. Zhou, J. Zhu, W. Xu, B. Dong and H. Song, Doping Lanthanide into Perovskite Nanocrystals: Highly Improved and Expanded Optical Properties, *Nano Lett.*, 2017, **17**, 8005–8011.
28 M. A. Becker, R. Vaxenburg, G. Nedelcu, P. C. Sercel, A. Shabaev, M. J. Mehl, J. G. Michopoulos, S. G. Lambrakos, N. Bernstein, J. L. Lyons, T. Stöferle, R. F. Mahrt, M. V. Kovalenko, D. J. Norris, G. Rainò and A. L. Efros, Bright triplet excitons in caesium lead halide perovskites, *Nature*, 2018, **553**, 189–193.
29 M. C. Brennan, J. E. Herr, T. S. Nguyen-Beck, J. Zinna, S. Draguta, S. Rouvimov, J. Parkhill and M. Kuno, Origin of the Size-Dependent Stokes Shift in $CsPbBr_3$ Perovskite Nanocrystals, *J. Am. Chem. Soc.*, 2017, **139**, 12201–12208.
30 W. Wu, W. Liu, Q. Wang, Q. Han and Q. Yang, Temperature-dependent photoluminescence of pure and Mn-doped $CsPbCl_3$ nanocrystals, *J. Alloys Compd.*, 2019, **787**, 165–172.
31 A. Ishii and T. Miyasaka, Sensitized Yb^{3+} Luminescence in $CsPbCl_3$ Film for Highly Efficient Near-Infrared Light-Emitting Diodes, *Adv. Sci.*, 2020, **7**, 1903142.
32 G. Pan, X. Bai, D. Yang, X. Chen, P. Jing, S. Qu, L. Zhang, D. Zhou, J. Zhu, W. Xu, B. Dong and H. Song, Doping Lanthanide into Perovskite Nanocrystals: Highly Improved and Expanded Optical Properties, *Nano Lett.*, 2017, **17**, 8005–8011.
33 X. Zhang, Y. Zhang, X. Zhang, W. Yin, Y. Wang, H. Wang, M. Lu, Z. Li, Z. Gu and W. W. Yu, Yb^{3+} and Yb^{3+}/Er^{3+} doping for near-infrared emission and improved stability of $CsPbCl_3$ nanocrystals, *J. Mater. Chem. C*, 2018, **6**, 10101–10105.
34 P. Dorenbos, Lanthanide 4f-electron binding energies and the nephelauxetic effect in wide band gap compounds, *J. Lumin.*, 2013, **136**, 122–129.
35 G. Kresse and J. Furthmuller, Efficient iterative schemes for ab initio total-energy calculations using a plane-wave basis set, *Phys. Rev. B: Condens. Matter Mater. Phys.*, 1996, **54**, 11169–11186.
36 C. Adamo and V. Barone, Toward reliable density functional methods without adjustable parameters: The PBE0 model, *J. Chem. Phys.*, 1999, **110**, 6158–6170.
37 B. Kang and K. Biswas, Exploring Polaronic, Excitonic Structures and Luminescence in $Cs_4PbBr_6/CsPbBr_3$, *J. Phys. Chem. Lett.*, 2018, **9**, 830–836.